energies

MDPI

Article

A Comprehensive Experimental Investigation of NO_x Emission Characteristics in Hydrogen Engine Using an Ultra-Fast Crank Domain Measurement

Mohamed Mohamed [1], Xinyan Wang [1], Hua Zhao [1], Mark Peckham [2], Jonathan Hall [3] and Changzhao Jiang [1,*]

[1] Centre for Advanced Powertrain and Fuels, Brunel University London, Uxbridge, London UB8 3PH, UK; mohamed.mohamed@brunel.ac.uk (M.M.)
[2] Cambustion Ltd., Cambridge CB1 8DH, UK; msp@cambustion.com
[3] Mahle Powertrain Ltd., Northampton NN5 5TZ, UK
* Correspondence: changzhao.jiang@brunel.ac.uk

Abstract: Adopting zero-carbon fuels, like hydrogen, can significantly reduce environmental harm and pave the way for a decarbonised trajectory with zero carbon emissions. The hydrogen internal combustion engine (ICE) technology has demonstrated its reliability and capacity to seamlessly integrate into the current ICE platform, originally designed for diesel and gasoline operation. The direct utilisation of pure hydrogen eradicates steady-state carbon dioxide and hydrocarbon emissions. It is important to highlight that efforts to comprehend and comprehensively tackle NO_x emissions are underway. A comprehensive study was carried out to assess the NO_x emissions for a hydrogen ICE with different injection modes from gasoline. The study involved varying the relative air-to-fuel ratio (AFR) from stoichiometric to the lean-burn limit in a boosted spark ignition (SI) engine fuelled with gasoline or hydrogen. A fast NO_x emissions analyser was employed to measure the instantaneous NO and NO_2 emissions in the engine exhaust. The study provides a detailed analysis of NO_x emissions, including steady-state averaged emissions, average crank angle domain NO_x distribution and emissions, in-cylinder pressure analysis, as well as time and cycle analyses of NO_x emissions' temporal and cyclic variations. The primary discovery was that NO_x emissions are almost zero between lambda 2.75 and 3.7, and hydrogen produces 13.8% less NO_x emissions than gasoline at stoichiometric operation. Finally, the full NO_x time analysis revealed that the consistency of NO_x emissions is higher with hydrogen than with gasoline by using a novel approach by identifying the coefficient of variation of the NO_x emission of each cycle.

Keywords: hydrogen ICE; NO_x emissions; ultra-fast measurement

Citation: Mohamed, M.; Wang, X.; Zhao, H.; Peckham, M.; Hall, J.; Jiang, C. A Comprehensive Experimental Investigation of NO_x Emission Characteristics in Hydrogen Engine Using an Ultra-Fast Crank Domain Measurement. *Energies* **2024**, *17*, 4141. https://doi.org/10.3390/en17164141

Academic Editor: Ashok Vijh

Received: 3 July 2024
Revised: 1 August 2024
Accepted: 5 August 2024
Published: 20 August 2024

1. Introduction

Petrol and diesel, which are traditional fuels derived from petroleum, continue to play a major role in transportation as a fuel source. Nevertheless, the emissions produced by these fuels, such as carbon monoxide (CO), hydrocarbons (HC), and nitrogen oxides (NO_x), are worrisome. In addition, hydrocarbon fuels emit greenhouse gases (GHG), such as carbon dioxide (CO2), which are recognised for their role in causing global warming and climate change. Consequently, regulatory authorities and governments worldwide have recently modified their targets for reducing carbon emissions. Consequently, strict pollution restrictions have been universally enforced for passenger and light commercial vehicles. As an illustration, the United States of America (USA) has enacted Executive Order 14037 to ensure that 50% of newly manufactured passenger automobiles and light-duty vehicles can operate without emitting any CO_2 by the year 2030. Similarly, the European Union has implemented Regulation (EU) 2023/851, which mandates that only cars with zero emissions (ZEV) will be available for purchase starting in 2035. The urgent need to decrease tailpipe emissions is propelling the advancement of alternate remedies [1,2].

NO_x, primarily generated from combustion processes, has substantial environmental effects and wide-ranging ramifications. NO_x emissions are a significant factor in air pollution, creating ground-level ozone and fine particulate matter. These pollutants have serious implications for human health, as highlighted by studies conducted by Huang et al. and Lelieveld et al. [3,4]. In addition to directly impacting air quality, NO_x emissions can cause nitrogen deposition in ecosystems, alter soil chemistry, and disturb nutrient cycles. Deposing acidic substances can result in soil acidification and cause changes in microbial communities, which can impact plant health and biodiversity [5,6]. In addition, NO_x emissions contribute to the accumulation of atmospheric nitrogen, which causes eutrophication in aquatic ecosystems and poses risks to water quality and aquatic biodiversity. The cumulative findings from these studies emphasise the diverse and wide-ranging effects of NO_x emissions on land- and water-based ecosystems, emphasising the necessity for efficient approaches to reduce their negative consequences [7,8].

Adopting zero-carbon fuels, like hydrogen, can significantly reduce environmental harm and pave the way for a decarbonised trajectory with zero carbon emissions. The hydrogen internal combustion engine (ICE) technology has demonstrated its potential and capacity to seamlessly integrate into the current ICE platform, originally designed for diesel and gasoline operation. The direct utilisation of pure hydrogen eradicates steady-state carbon dioxide and hydrocarbon emissions. It is important to highlight that efforts to comprehend and comprehensively tackle NO_x emissions are still in progress.

The transition towards achieving zero-carbon emissions for internal combustion engine (ICE) technology necessitates a shift from fossil fuel-based to non-carbon fuels. Biofuels, which can be used as drop-in fuels, offer a promising solution with higher CO_2 life-cycle emission reduction rates. However, it is worth noting that the tailpipe emissions associated with biofuels are nearly on par with those of fossil fuels [9,10]. Premade fuel mixtures containing both alcohol and gasoline are recognised for their ability to effectively decrease overall vehicle emissions, leading to a reduction in particulate matter emissions. However, the NO_x emissions from spark-ignited (SI) engines have varying responses depending on the engine's powertrain setup [11,12]. Research studies indicate that ethanol and methanol exhibit superior performance to gasoline engines in terms of thermal efficiency in various operating conditions. The improvement in thermal efficiency is more evident at higher loads and power outputs. The high knock resistance of ethanol and methanol enables more advanced combustion timing, eliminating the necessity for excessive fuelling under full load and power operations. This is due to the higher latent heat and lower air-fuel ratio of alcohol fuels, contributing to a higher knock resistance [13,14].

Prior solutions have made strides in reducing carbon emissions, but carbon-free fuels, such as ammonia (NH_3) and hydrogen (H_2), are necessary to eliminate emissions fully. These fuels lack carbon atoms in their chemical makeup and can ensure zero carbon emissions throughout their life cycle when sourced from renewable sources. This provides the opportunity to significantly reduce the generation of HC, CO, and CO_2 during the combustion process. However, partial burning of lubricating oil in the combustion chamber may still produce some of these emissions [15–17].

Ammonia is a commonly used fertiliser that has been suggested as a carbon-free fuel option for internal combustion engines. However, the current ammonia production can have detrimental environmental impacts, so various green ammonia production methods are being explored. While ammonia use as a fuel has benefits, it also poses some drawbacks. Its utilisation in combustion systems necessitates a high boost pressure and compression ratio or a combination with hydrogen. Dual-fuel compression-ignition engines can use both diesel and ammonia. However, ammonia combustion produces exhaust NO_x and unburned NH_3, necessitating the implementation of after-treatment systems. Ammonia is a more viable option for stationary or maritime engine applications. Improving the quality of direct fuel replacement combustion would need more research and development [18–21].

Hydrogen usage in ICE offers several advantages besides eliminating carbon emissions. Minor modifications are sufficient to implement H_2 in ICEs, and its high-octane

number (130 or higher) and high auto-ignition temperature provide high resistance to end-gas autoignition combustion. The combustion stability is improved due to the faster burning rate of hydrogen than gasoline. H_2's high diffusion coefficient also promotes the homogeneous mixture of air and fuel. H_2's broader flammability range allows for leaner operation without increased ignition energy, decreasing the probability of abnormal combustion such as backfire, pre-ignition, and surface ignition. The leaner operation also significantly reduces engine-out NO_x emissions with higher air–fuel equivalence ratio (λ) values above 2. Achieving the desired power density and higher engine load requires an ultra-lean mixture and a high level of intake-boosting air. However, leaner combustion could result in lower combustion efficiency by producing more unburned fuel, lowering thermal efficiency and exhaust gas temperature (EGT), negatively impacting the available enthalpy for driving turbochargers [22–27].

Hydrogen is a promising alternative fuel to replace gasoline in ICE due to its zero-carbon emissions and better performance. However, using hydrogen as fuel poses some challenges. One of the main challenges is the higher air-to-fuel ratio of 34 compared with 14.6 for gasoline, which means more air is needed to combust hydrogen, resulting in higher pumping mean effective pressure (PMEP). The higher flame speed of hydrogen leads to a fast burn rate, which causes a higher pressure rise rate and limits the engine's load. Additionally, hydrogen combustion produces NO_x emissions, which are harmful to the environment. One of the main solutions to reduce NO_x emissions is to operate the engine on the lean side, which means running the engine at lambda 2.75 to 3.5 to lower the burn speed, which significantly drops the pressure rise rate and the NO_x. However, operating on the lean side presents a new challenge in control and calibration, and new boosting solutions may be necessary to adopt that. On the other hand, operating the engine at the stoichiometric region provides safety concerns, as H_2 port fuel injection (PFI) can backfire in the intake, which leaves the only way to operate at the stoichiometric combustion associated with H_2 direct injection (DI) [25,28–32].

The previous analyses of NO_x emissions have not included direct comparisons between hydrogen and gasoline combustion in the same engine and their values at various lambda values. Additionally, there has been little work reported on the direct comparison between the DI and PFI hydrogen engine operations. Furthermore, most previous studies have been conducted on time-averaged NO_x emissions. Therefore, a thorough NO_x emissions assessment was conducted in this study across three distinct phases. In the first part, the ensemble-averaged NO_x emissions over 300 cycles were determined and compared between H_2 DI and PFI operations and the DI gasoline operation. The analysis of instantaneous NO and NO_2 emissions was then extended to the crank domain with a resolution of 0.25 crank degrees. Finally, the cyclic variation of NO_x emissions was analysed for the PFI/DI hydrogen engine operations and the DI gasoline engine operation with correlations drawn of each exhaust stroke's NO_x emissions vs. cylinder pressure parameters (similar to [32]).

2. Experimental Setup

In this specific setup, incorporating a pressure hydrogen line into two separate injection positions while maintaining high safety standards posed a significant challenge. One of the most pressing issues with hydrogen lies in establishing a new risk assessment for the hydrogen supply line to determine the location of the hydrogen source. Unlike automotive and transportation applications, hydrogen use in the test cell requires a permanent and isolated location for safely storing hydrogen bottles without causing any leakage Risk. The test cell needed to address potential hazards, so the solution involved securely isolating and ventilating the bottles outside the test cell. To accomplish this, the bottles were placed in a partially enclosed space surrounded by fire shields without a ceiling. It was also beneficial to position all supply line accessories outside the test cell, including pressure regulators, sensors, flow meters, and shutdown valves. This practice reduced the risk of leaks within the test cell by limiting the number of connections. An additional ATEx ventilation system

with a flexible hood was installed in the test cell to optimise air recirculation. The engine was equipped with a hydrogen sensor connected to an automated shutdown Programmable Logic Controller (PLC) system to respond automatically to hydrogen levels exceeding 3% v/v by interrupting the hydrogen supply line and purging it with nitrogen. The automated shutdown PLC system also activates in the event of backfire detection during Port Fuel Injection (PFI) usage and in the event of hydrogen leakage into the crankcase, triggering the crankcase ventilation system to prevent hydrogen accumulation. Implementing an automated PLC system, along with a double vacuum tubing system, addressed the issue of potential hydrogen pipeline leaks. The double vacuum tube connected to the pipeline ensures that any leaked hydrogen remains confined within the outer tube and is subsequently purged out by nitrogen. A pressure sensor on the double vacuum tube is linked to the PLC to activate the nitrogen purging system.

2.1. Engine Setup

In this study, a spark ignition (SI) single-cylinder engine provided by MAHLE Powertrains/(Northampton, UK) was utilised to evaluate the performance and emissions of hydrogen in two different injection configurations: central direct injection and port fuel injection. The engine is equipped with a MAHLE adaptable electronic control unit (ECU), which facilitates a seamless transition between hydrogen and gasoline operation on a single engine, requiring minimal adjustments to the control system. The engine utilised DI-CHG10 injectors manufactured by Phinia for both DI and PFI, enabling hydrogen injection ranging from 2 to 10 bar in the PFI system and 10 to 40 bar in the DI system. The crankcase ventilation system has been altered to address potential hydrogen-related risks. This modification involves implementing a forced ventilation system, which includes a hydrogen sensor in the feedback loop. If the hydrogen concentration in the crankcase exceeds 4% v/v, the system will automatically reduce the hydrogen supply, as per Figure 1. The upgraded system has a built-in mechanism that keeps track of the piston rings' condition. It features fully adjustable valve timing for both the intake and exhaust cams, allowing the freedom to pick the ideal overlap configuration for each injection system. Moreover, the engine control unit (ECU) permits the injection timing and pressure to be tweaked, facilitating the modification of the beginning or end of the injection process as required. The engine has a self-sufficient boosting system that can generate a maximum boost pressure of 4 bar and an externally controlled heater with a PID regulator that accurately controls the intake pressure and temperature. The main engine specifications are in Table 1.

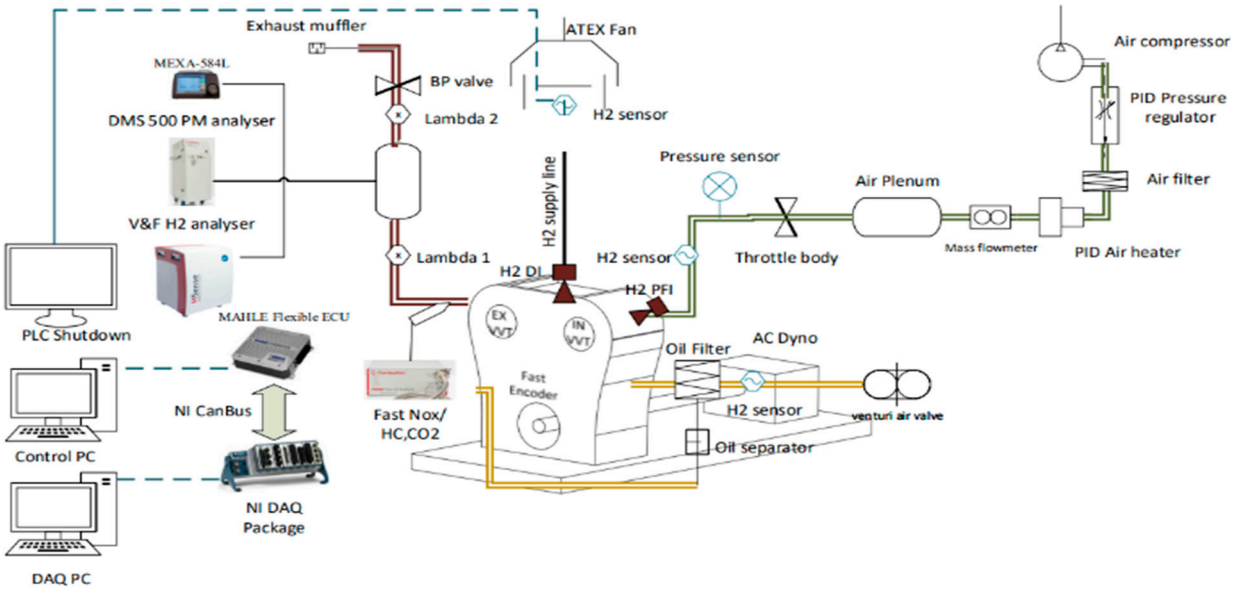

Figure 1. Schematic of H2 ICE test cell setup [33].

Table 1. Engine specifications [34].

Configuration	Single Cylinder
Displaced volume	400 cc
Stroke × Bore	73.9 mm × 83 mm
Compression Ratio	11.3:1
Number of Valves	4
Exhaust Valve Timing	EMOP (Exhaust Maximum Opening Point) 100 early open exhaust valve −140 late close exhaust valve °CA BTDC, 11 mm Lift, 278 °CA Duration
Inlet Valve Timing	IMOP (Intake Maximum Opening Point) 80 early open intake valve −120 late close intake valve °CA ATDC, 11 mm Lift, 240 °CA Duration
Injection System	Central Direct Injection outwardly opening spray $\leq$ 200 bar for gasoline and up to 40 bar for H_2 PFI injector up to 10 bar
Injection Control	MAHLE Flexible ECU (MFE)
Spark location	CDI = Top central toward exhaust valves SDI = Top central of 4 valves
Spark Plug Type	Surface Discharge Type (NGK HR10)
Combustion Chamber configuration	Tumble-based (NDRT 0.7 @ max lift)

One of the primary obstacles that requires clarification pertains to the operational limitations of the engine. The single-cylinder engine can operate up to 5000 rpm and attain a maximum peak in-cylinder pressure of 120 bar. However, this restricts its operation at exceedingly high loads, with a pressure rise rate of six bars per crank degree, in order to prevent damage to the timing chain. Additionally, the maximum exhaust temperature is 750 degrees Celsius, and the hydrogen slip limit must not exceed 6000 parts per million (ppm) to prevent a hydrogen fire in the exhaust line, which the heated lambda sensors in the line could cause.

2.2. Fuel System and Proprieties

The hydrogen supply system starts at the hydrogen containers in the isolation chamber. It then passes through the initial control panel, which adjusts the hydrogen pressure from the bottle's internal pressure to a standardised 40 bar. After that, it passes through a pressure sensor and a safety solenoid valve before reaching the hydrogen flowmeter. Placing the hydrogen flowmeter downstream of the initial stage mainly reduces any potential impact on the final pressure delivered to the injector caused by pressure drops induced by the flowmeter. In the next stage, the regulator lowers the pressure within the 2 to 30 bar range, improving accuracy. The second panel is equipped with an extra pressure sensor and a safety solenoid valve, which isolate the line and reduce hydrogen slips if there is hydrogen leakage. Upon entering the test cell, the hydrogen line is enclosed within an additional tube that maintains a vacuum to prevent any hydrogen leakage to the external environment. The entire tube includes a pressure sensor that activates an automatic nitrogen purge to ensure complete isolation of the hydrogen line. This setup is shown in Figure 2.

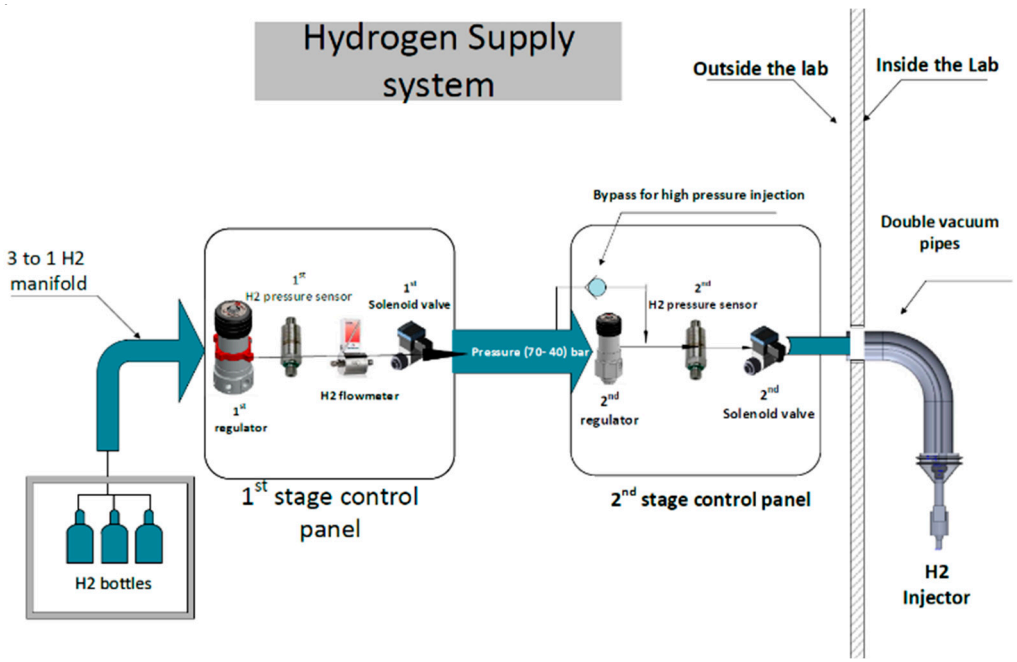

Figure 2. H2 supply line.

2.3. Emission Analysers

An ultra-fast response NO_x analyser was used for these experiments (Cambustion CLD50 fast NO and NO_2 analyser). This instrument differs from standard analysers because it had a response time of approximately five milliseconds in the configuration deployed in these experiments and sensitivity to tens of parts per billion. It is, therefore, ideally suited for measuring transient NO and NO_2 in the exhaust of H_2 combustion engines where very low NO_x levels can be achieved but where transients between operating conditions can cause sudden high "spikes" of NO_x [35].

Nitric oxide (NO) was measured with a chemiluminescence detector (CLD), and nitrogen dioxide (NO_2) was measured with laser-induced fluorescence (LIF). This direct method of NO_2 measurement differs from conventional NO_x analysers, where the sample is usually passed through a converter, and the difference between direct NO and the resulting total NO_x via the converter is calculated to assume the NO_2, a much slower process.

The ultra-fast response time was particularly appropriate for the measurement of cycle-resolved data, where such measurement would not have been possible with conventional slower analysers. Finally, the exhaust pipe is connected to the V&F emission analyser for hydrogen slip measurements. Table A1 in the appendix shows the full details of the equipment used, including the measurement range and error percentage.

2.4. DAQ System

The number of the input channels is 138 signals from the test cell. However, the sampling rate required for each sensor depends on the sensor's priority and the reading's value. In-cylinder, intake, and exhaust pressure sensors are required to provide a sample in the crank angle domain compared to other sensors operating in the regular time domain. Based on that, the NI cards were a hybrid selection between fast and standard USB NI cards that can auto synchronise in the NI-based combustion analyser Valieteck. Also, the NI to canbus communication card transfers signals from the ECU, as shown in Figure 3.

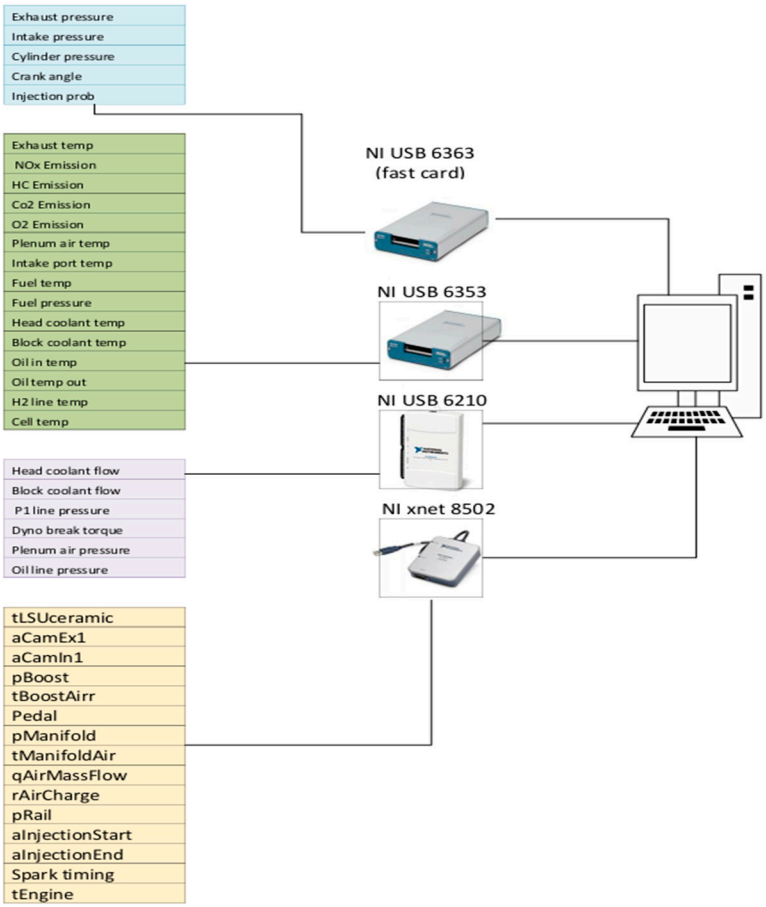

Figure 3. Schematic of DAQ system.

Cyclic variability in an internal combustion engine causes periodic torque production and emissions fluctuations. To assess the stability of combustion, the coefficient of variation of indicated mean effective pressure (COV_{IMEP}) is often used. Although the cyclic changes cannot be eliminated, they can be regulated to maintain steady engine performance using Equation (1).

$$COV_{IMEP}(\%) = \frac{\sqrt{\frac{\sum_{i=1}^{n}(IMEP_1 - IMEP_{mean})^2}{n-1}}}{IMEP_{mean}} \quad (1)$$

3. Test Methodology

The research examines the NO_x discharge properties of hydrogen and traditional gasoline combustion engines by focusing on the NO_x formation process and its reliance on the λ. The engine was operated at a fixed load and speed of 10 bar IMEP and 2000 RPM, representing a mid-load and speed point and varying the lambda values from lambda = 1 to the maximum lean points of each fuel. The intake temperature was fixed at 38 °C, as a dryer was connected to the intake line, which provided zero humidity in the intake air; therefore, the air was heated to 38 degrees to overcome this advantage and make the results representative of the three-cylinder engine model, and both oil and water temperatures were kept at 90 °C. The intake cam maximum opening was set at 97 degrees after the gas exchange top dead centre (ATDCg), and the exhaust cam was fixed at 102 degrees before the gas exchange top dead centre (BTDCg). The injection timing and pressure were optimised for each fuel to ensure that both fuels ran at the maximum brake torque (MBT) point. This study examined the engine performance characteristics and constraints of hydrogen compared with baseline gasoline fuel under identical engine configurations,

intake temperature, and air humidity conditions. Table 2 shows the operation conditions at test points.

Table 2. Engine test conditions.

Engine Parameters	Unit	λ Sweep Test
Engine speed	rpm	2000
Engine load	kPa	1000
λ	-	SWEEP (1 to 3.8) with step change of 0.2
Intake Cam positions	ATDCg	97
Exhaust Cam positions	BTDCg	102
Start of injection H2 DI	BTDCf	150
Start of injection gasoline DI	BTDCf	300
Injection pressure H2 DI	kPa	3000
Injection pressure gasoline DI	kPa	100,000
Intake air temperature	°C	38

4. Results and Discussion

The results are presented in two stages: first, we present the results associated with PFI and GDI fuelling during lambda sweeps, and second, the study evaluates NO_x emissions within the average crank angle domain to demonstrate the average levels of NO_x emissions observed across 300 cycles, including analysing NO_x emissions using in-cylinder data in the time domain enables the observation of fluctuations in NO_x levels over a specific period.

4.1. Impact of Lambda on Average NO_x Emissions

This section presents a study exploring the performance and NO_x emission characteristics of H_2 ICE compared to baseline gasoline engines across a broad range of relative AFRs. All operation points at different relative AFRs were fixed at 50% burn of 8 degrees ATDCf to maintain MBT. With cam timing fixed for each fuel, the scavenging effect from the overlap was bypassed. Figure 4 shows the Indicated Thermal Efficiency (ITE) of central DI H2 and gasoline fuel over various lambda values up to the limits of the COV_{IMEP}. The results demonstrate the vast relative λ map of hydrogen compared with the narrow range of gasoline operations. Hydrogen DI operates from stoichiometric combustion to a maximum relative AFR of 3.8, with COV_{IMEP} below 1.6%. On the other hand, gasoline DI managed to operate up to a lambda of 1.6 at 2% COV and a maximum lambda of 1.8 at 4.2% COV. The ITE results reveal that hydrogen has a higher ITE of 41% compared with gasoline's 37.4% at the leanest operating points. The lower ITE of hydrogen at stoichiometric operations is due to a higher hydrogen slip from the exhaust system. Also, the burn characteristics of the hydrogen fuel as the hydrogen flams speed are much higher than the gasoline, with results in a massive pressure rise rate that forces the operator to retard the spark timing up to 11 CAD ATDCf, which results in a sudden drop of the ITE, as pre previous study [36].

It should be noted that the engine was designed and built for gasoline fuel and adopted hydrogen without any modifications. Also, it was observed that the value of the H_2 slip increased with leaner combustions. However, the H_2 slip remained under the threshold.

The data in Figure 5 depict the mean NO_x emission captured from the fast NO_x emission analyser in the exhaust port while varying the relative λ for hydrogen DI and PFI compared to gasoline DI. The key finding indicates that hydrogen results in a negligible NO_x emission above lambda 3, with NO_x levels dropping below 50 ppm from lambda 2.75. As a result, an exponential increase in NO_x emission is observed when lambda reduces from 2.5 to 1.4 with peak NO_x emissions captured.

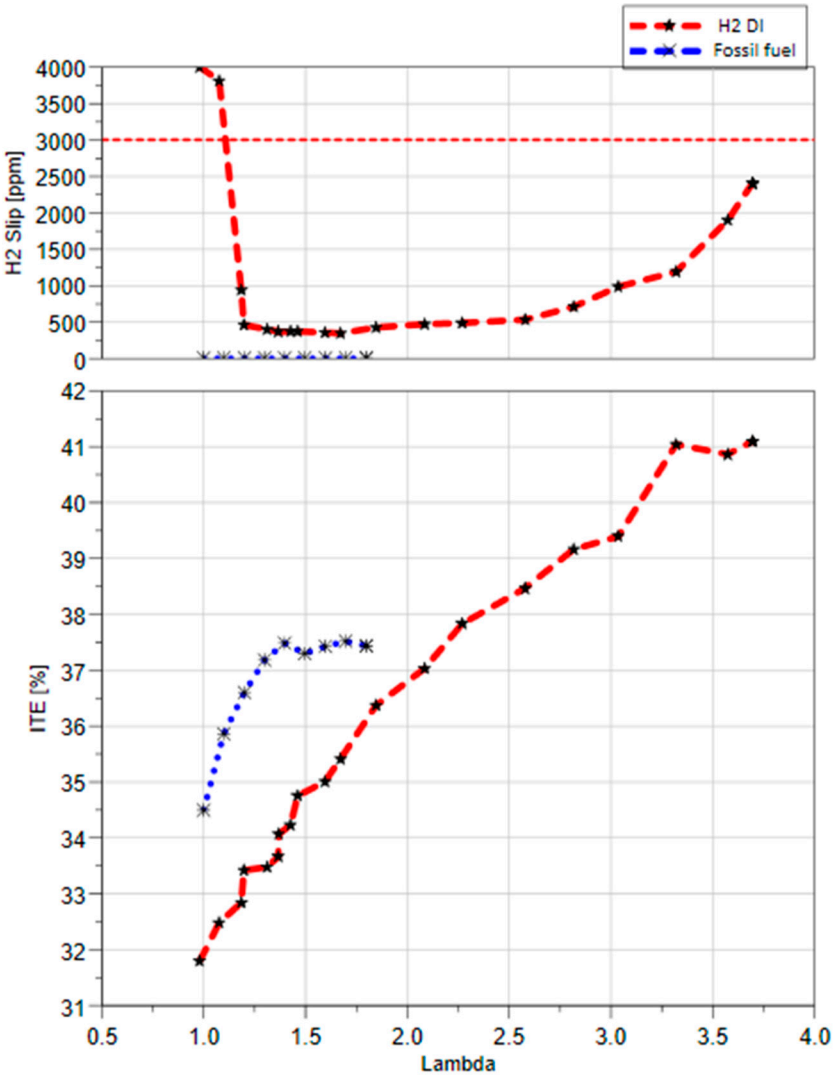

Figure 4. Hydrogen slip in the exhaust and Indicated thermal efficiency for gasoline vs. hydrogen at different lambda.

The graph displays a slightly lower NO_x emission for the hydrogen PFI system compared with the hydrogen DI system due to the complete burn and the higher thermal efficiency of the DI system, which results in a higher in-cylinder gas temperature that causes higher NO_x at the same load. However, at lambda 2.75, the difference is almost negligible, and at lambda 3, the NO_x emissions fall below 10 ppm for both hydrogen injection systems. Additionally, the NO_x emissions for the PFI system match those of the DI at a lambda of 1.5 where the backfire starts appearing in the intake line for the PFI.

Finally, a comparison of NO_x emissions between the direct injection systems of hydrogen and gasoline reveals that at stoichiometric combustion operations, the NO_x emission is lower in hydrogen than gasoline by almost 41% due to H_2 slip at lambda 1, which results in less thermal efficiency and lower peak cylinder temperature. The study also observed that the lambda point of the peak NO_x emissions of each fuel was different, with gasoline at lambda 1.3 and hydrogen at lambda 1.38, influenced by the fuel properties that directly affect the NO_x formation mechanisms.

This section aimed to identify the NO_x emissions characteristics and the ITE of both hydrogen and gasoline engines. The data presented indicate the average NO_x emissions at each testing point.

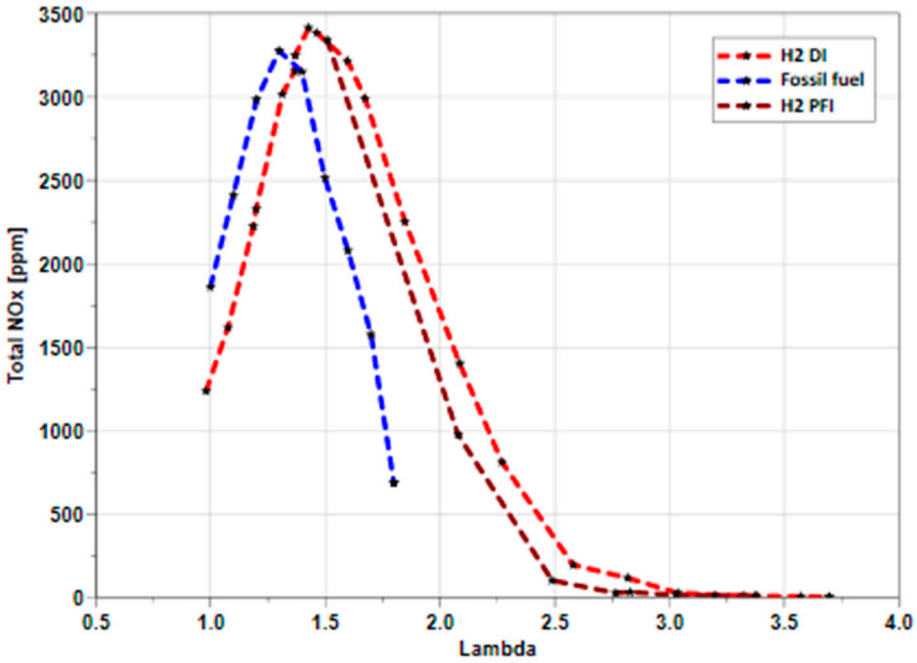

Figure 5. NO_x emission for gasoline and hydrogen at different lambda values with fixed load and speed of 10 bar IMEP and 2000 rpm.

4.2. Analysis of NO_x Emissions in the Crank Angle Domain

This section presents the NO_x emission data and in-cylinder pressure in the crank angle domain to illustrate the NO_x emission characteristics and distribution. Additionally, the study breaks down the NO_x emissions to analyse the distribution of NO and NO_2 separately over the crank angle domain. Furthermore, the study directly compares the NO_x emission and in-cylinder pressure under very lean operation conditions by comparing the hydrogen DI and PFI systems. The aim is to provide an in-depth understanding of NO_x emission behaviour and distribution in the crank angle domain, which could help improve engine performance and develop emission control strategies. The presented results are the corrected results with the delay function as we built on the time delay function that consists of static delay, which represents the T90 response time of the equipment and the 1.2 m heated line length, plus the dynamic delay, which is calculated on the basis of the exhaust pressure and flowrate. This correlation shifts the start of the Nox generation with the exhaust valve opening to produce consistent NO_x measurements in the crank domain.

Figure 6 shows the NO and NO_2 emissions from the hydrogen DI system with a very lean combustion of lambda 3.3. The graph illustrates the distribution of NO and NO_2 in the crank angle domain and the averaged in-cylinder pressure over 300 cycles, representing the ensembled average. The results indicate that the NO_2 levels are approximately 4 particles per million (ppm). Meanwhile, NO emissions are below 2 ppm. The effect of the exhaust opening event is visible at around 170 degrees after the firing top dead centre (ATDCf), corresponding to the exhaust valve opening timing. At this operating point, the NO_2 emissions are higher than NO due to the higher error gain of NO_2. However, both NO and NO_2 values are within the measurement range, indicating that both emissions are negligible.

Figure 7 illustrates the relationship between these emissions and in-cylinder pressure at a lambda of 2.75, which is considered an optimum engine operating point due to a lower requirement of boosted air and minimum NO_x emission. The figure shows that hydrogen DI and PFI systems produced almost identical in-cylinder pressure. The location of the peak pressure of 6878 KPa is 6 degrees ATDCf. Notably, NO emissions account for 80% of the total NO_x emissions, while NO_2 only accounts for the remaining 20%.

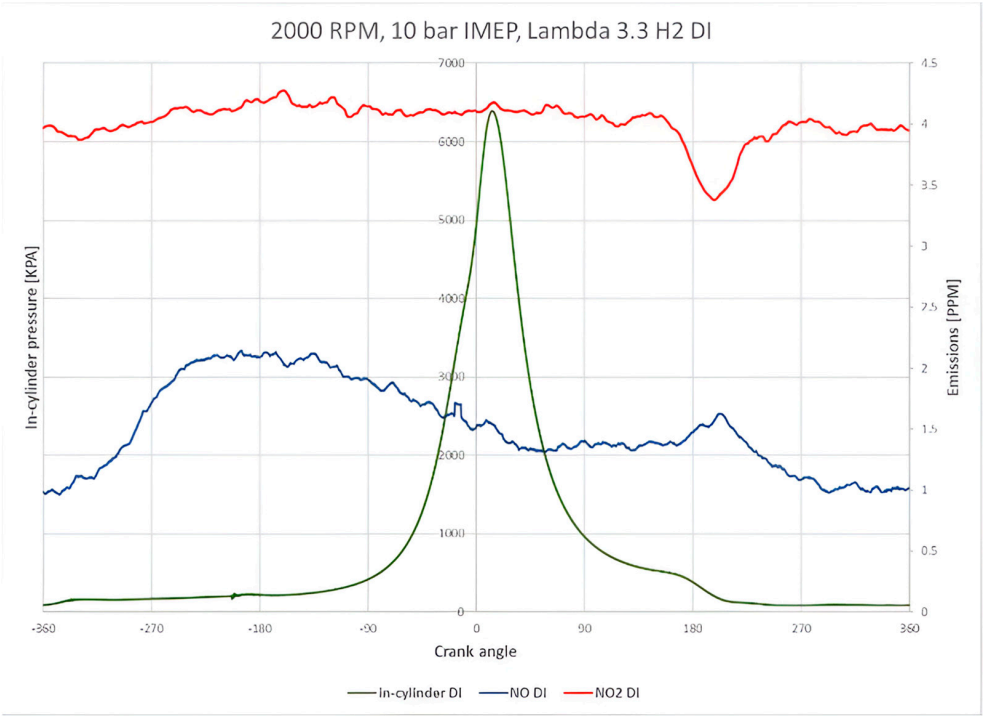

Figure 6. Averaged NO and NO_2 emissions for DI hydrogen in the crank angle domain at a lambda of 3.3.

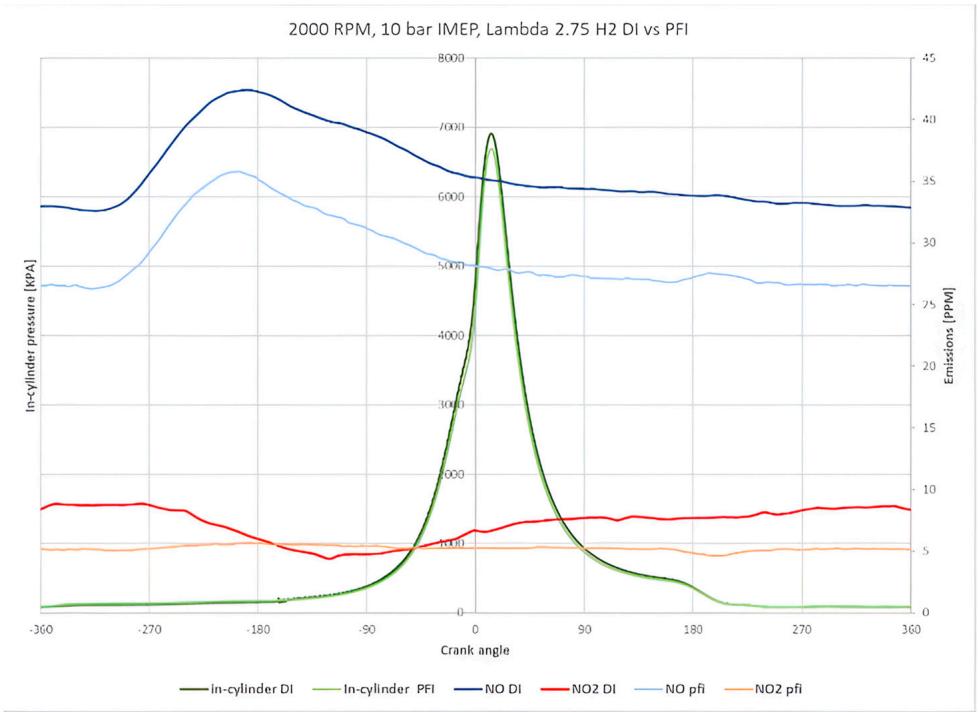

Figure 7. Averaged No and NO_2 emission for DI and PFI hydrogen in the crank angle domain at lambda value 2.75.

Furthermore, the results indicate that the DI system generates higher NO_x emissions than the PFI system by 14 ppm, suggesting a higher thermal efficiency. Interestingly, the distribution of NO across the crank angle domain shows a saturation on the exhaust opening side, and the peak of the NO is detected at the intake stroke. This delay occurred due to the overall low NO concentration.

Figure 8 illustrates the rapid NO and NO_2 emissions characteristics at a lambda of 1.5, which has the highest NO_x emissions, with the hydrogen DI system. The diagram depicts the significant NO spike occurring at 156 degrees ATDCf, which is a delay of around 5 degrees from the opening time of the exhaust valves. Additionally, it also shows that the location of the NO peak aligns with the exhaust valve opening peak as the measuring probe is mounted just behind the valve, which indicates that the delay function provides an accurate estimation of the system delay.

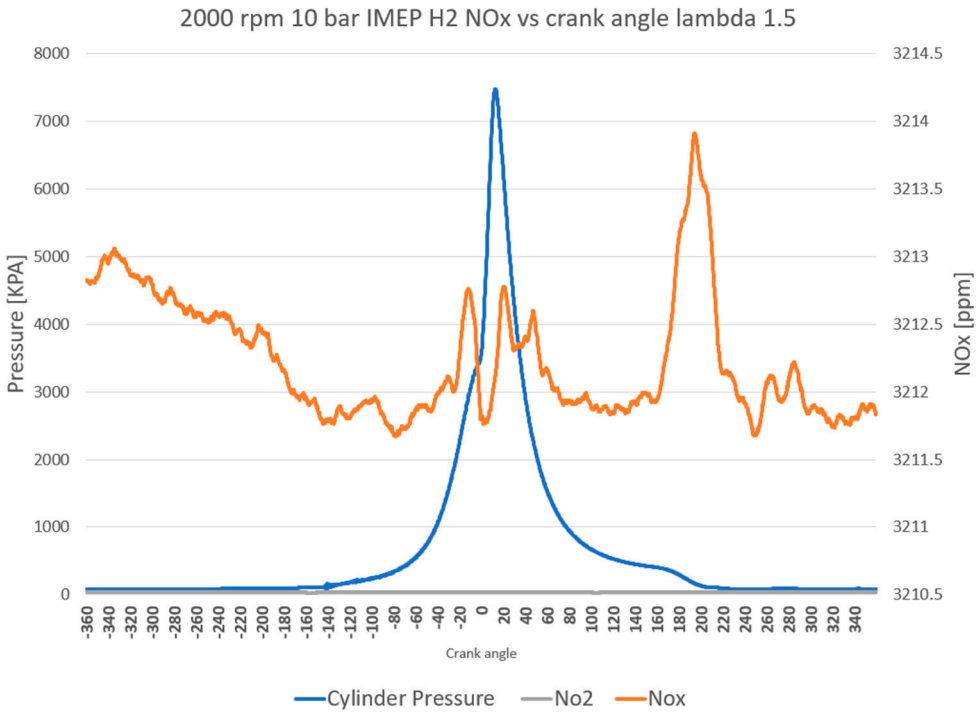

Figure 8. NO_x emission distribution for DI hydrogen in the crank angle domain at a lambda of 1.5.

These findings demonstrate the importance of carefully monitoring and adjusting spark timing to ensure safe and efficient engine operation.

Figure 9 directly compares NO_x emissions over the crank angle domain for the hydrogen and gasoline DI systems at lambda 1.3, where a peak of NO_x emissions was observed for gasoline fuel. The NO_x emissions for both fuels exhibit low fluctuation levels of less than 10% over the cycle. However, the NO_x emissions of hydrogen are 9.3% lower compared with those for gasoline. The in-cylinder pressure data reveal the operational differences between the two fuels. Gasoline exhibits a lower in-cylinder pressure of almost 1000 kPa than hydrogen. Furthermore, the retarding of spark ignition timing of hydrogen operation is indicated by the location of peak in-cylinder pressure, which is around 13 crank angle degrees after that of peak in-cylinder pressure for gasoline. This feature significantly impacts the ITE of the hydrogen DI system when operating at this lambda configuration.

Figure 10 displays the NO_x emissions across the crank angle domain for the hydrogen and gasoline systems at lambda 1, the stoichiometric ratio. The in-cylinder pressure indicates a significant retarding of spark ignition to nearly 5 degrees ATDCf for hydrogen to maintain the maximum pressure rise rate within the allowable limits. It is noteworthy that the NO_x levels of hydrogen operation are lower by 370 ppm than those of gasoline. Furthermore, the in-cylinder pressure highlights the difference in combustion characteristics, as hydrogen exhibits much higher in-cylinder pressure with a retarded ignition to ensure the engine operates within limits. The study underscores the criticality of the ignition timing and the fuel characteristics in managing NO_x emissions, particularly with hydrogen fuel.

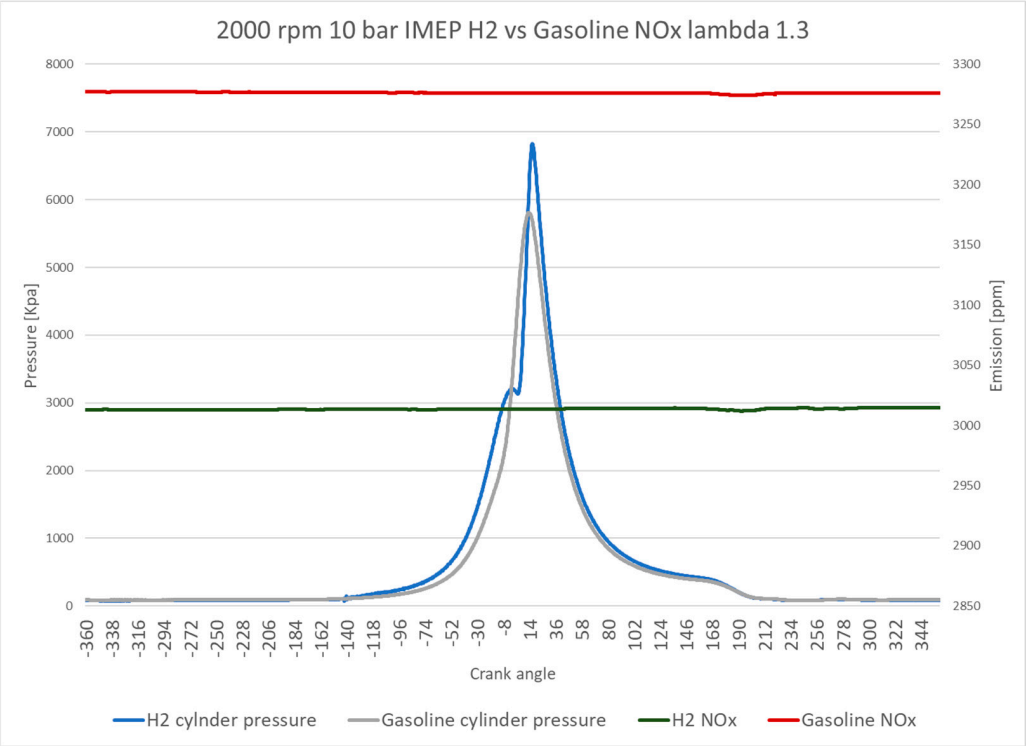

Figure 9. NO_x emission for DI hydrogen and DI gasoline and in-cylinder pressure traces in the crank angle domain at a lambda of 1.3.

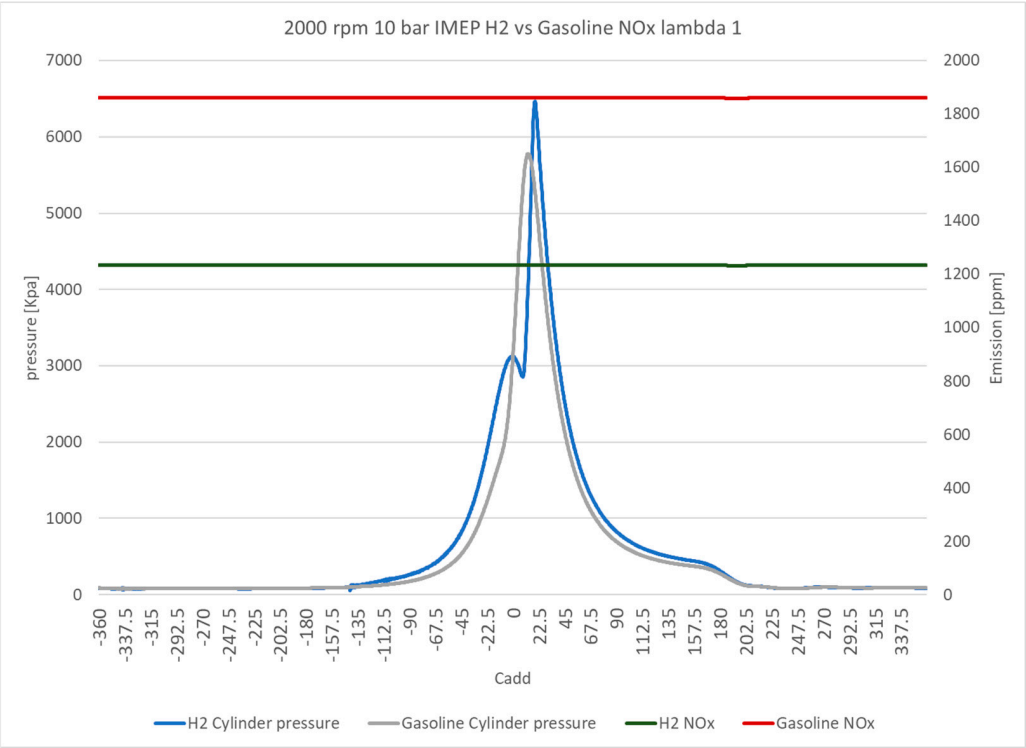

Figure 10. NO_x emissions for DI hydrogen and DI gasoline and in-cylinder pressure in the crank angle domain at a lambda of 1.

The analysis conducted in this study outlines NO and NO_2 emissions distribution across the crank angle domain. Additionally, the in-cylinder pressure data are presented, highlighting the differences between hydrogen and gasoline at varying relative AFRs. The

study further confirms the negligible NO_x emissions at lambda 3.3 and a direct comparison between hydrogen DI and PFI at lambda 2.75 with NO_x emissions around 50 ppm. Overall, the results demonstrate a comprehensive understanding of the NO and NO_2 emissions distribution and provide useful insights into the differences between hydrogen and gasoline fuels under different conditions.

4.3. Analysis of NO_x Emissions in the Time Domain

The performance and emissions of hydrogen and gasoline operations have been analysed in the previous sections by averaging 300 cycles. Additionally, the crank angle domain analysis shows the averaged data across 300 cycles. This section aims to analyse the cycle-to-cycle NO_x emissions characteristics to fully comprehend and understand the dependency of NO_x on other combustion parameters, such as the peak in-cylinder pressure and the engine cycle-to-cycle variations (CCVs).

In the time domain, the in-cylinder pressure and NO_2 emissions of 15 cycles at lambda 2.75 are shown in Figure 11. The data indicate that high NO and NO2 fluctuations are observed, though the engine Coefficient of Variation (COV_{IMEP}) was less than 0.6%. The NO emission shows minimal variation of 20 ppm, as the overall NO_x emissions at lambda 2.75 are close to zero. The location of the peak NO_x varies on the basis of cycle-to-cycle dynamics.

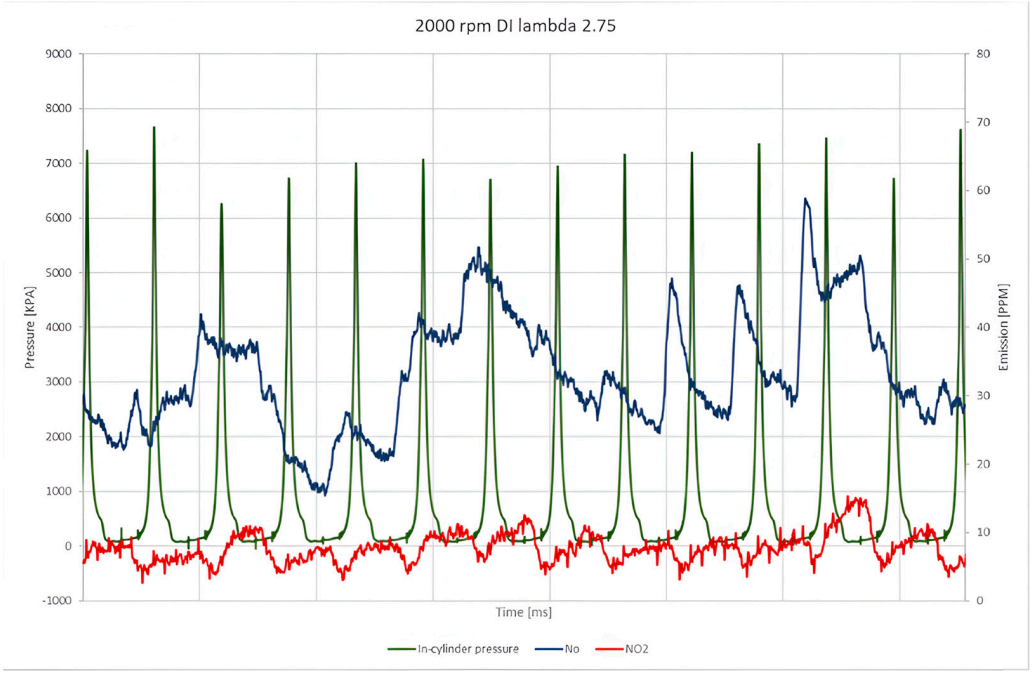

Figure 11. NO_x emission and in-cylinder pressure for DI hydrogen in the time domain at a lambda 2.75.

Figure 12 displays the average NO_x emissions over 200 cycles and the NO_x variations indicated by the COV_{NO_x}. Furthermore, both gasoline and hydrogen DI systems at a lambda of 1.3 are directly compared in Figure 12. The data demonstrate that hydrogen has constant NO_x emissions with minor oscillations of less than 0.5% on average. By contrast, gasoline has unstable NO_x emissions with higher levels of cycle-to-cycle variations, therefore greater COV_{NO_x}, as shown in Figure 12, and Equation (2) provides the COV_{NO_x} calculation.

$$COV_{NOx}(\%) = \frac{\sqrt{\frac{\sum_{i=1}^{n}(NOx_1 - NOx_{mean})^2}{n-1}}}{NOx_{mean}} \quad (2)$$

Figure 13 presents the peak in-cylinder pressure of each cycle against the NO_x emissions at a relative λ of 1.3. Though the COV_{IMEP} of both fuels is less than 1%, it is apparent that the variation of peak in-cylinder pressure in gasoline DI is significantly greater than

that in hydrogen DI. This is evidenced by the wider peak in-cylinder pressure distribution observed in gasoline DI. The figure also illustrates that hydrogen produced higher peak in-cylinder pressure with lower NO_x emissions.

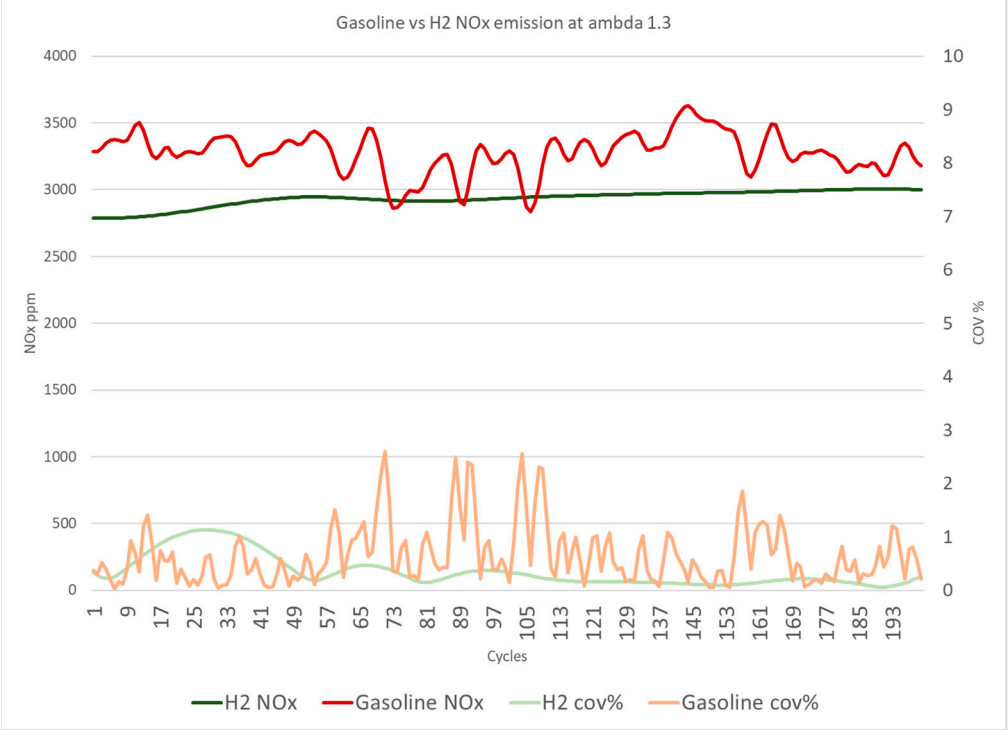

Figure 12. NO_x emission and NO_x variation for DI hydrogen and DI gasoline across 200 cycles at a lambda of 1.3.

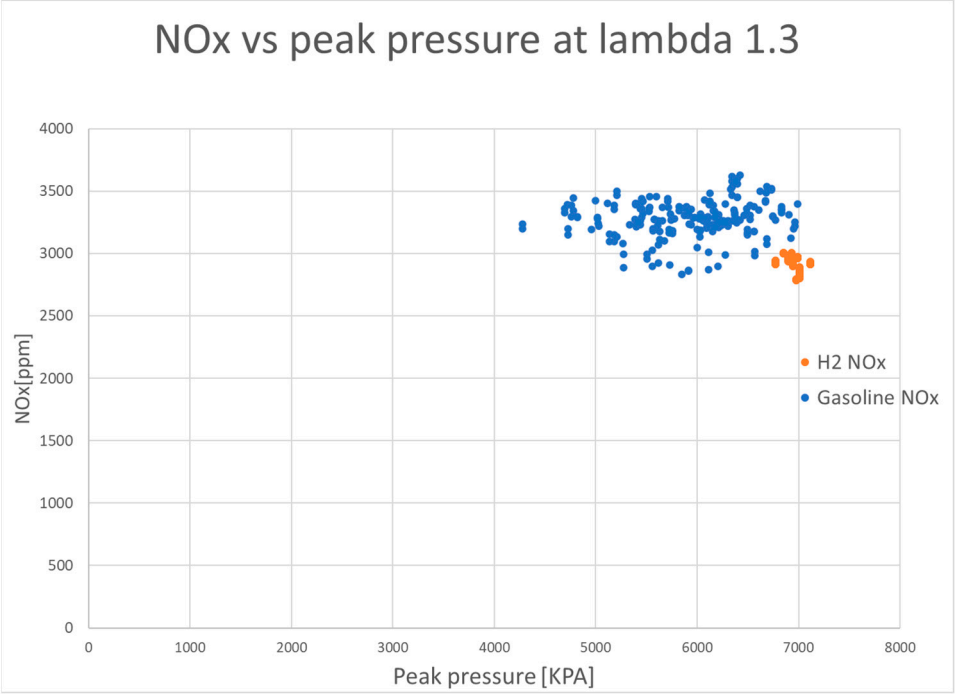

Figure 13. NO_x emission and peak cylinder pressure for hydrogen DI and gasoline DI at a lambda of 1.3.

Figure 14 depicts the NO_x emissions of gasoline and hydrogen DI at a lambda of 1. The results indicate that gasoline produced higher NO_x emissions and oscillation levels

than hydrogen. Although the engine is primarily designed and optimised to operate with gasoline as the primary fuel, hydrogen exhibits more stable NO_x emissions with less COV_{NO_x} per cycle and lower average NO_x levels.

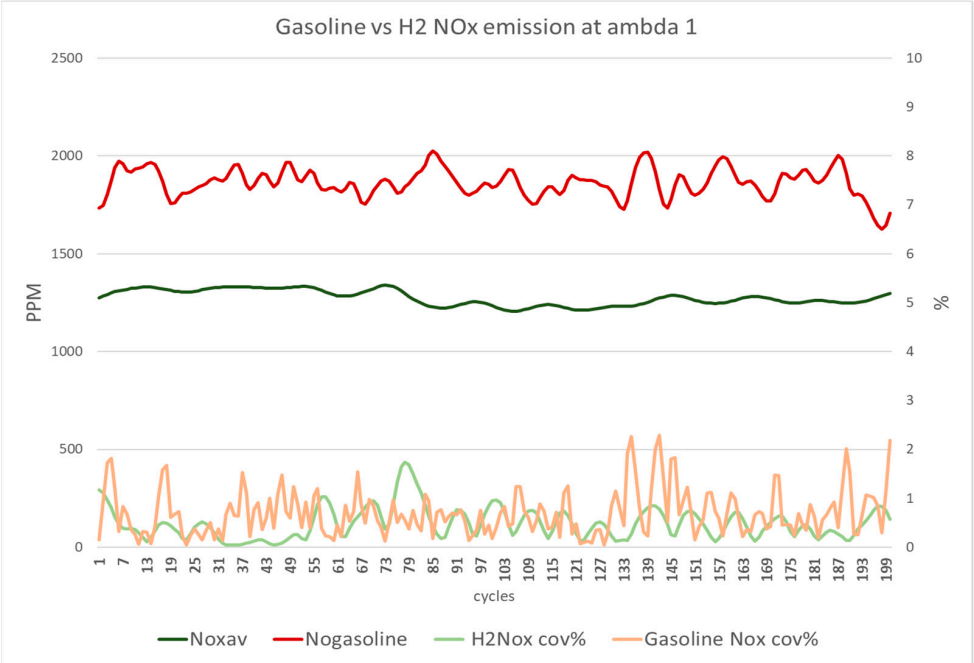

Figure 14. NO_x emission and NO_x variation for DI hydrogen and DI gasoline in 200 cycles at a lambda of 1.

Figure 15 displays the in-cylinder peak pressure in relation to NO_x emissions for 200 cycles under stoichiometric conditions. The data indicate that gasoline exhibits higher in-cylinder pressure variation and a greater oscillation of NO_x emissions than hydrogen. Conversely, hydrogen demonstrates a stable peak in-cylinder pressure and lower NO_x emissions. The results provide clear evidence for the benefits of hydrogen fuel in reducing NO_x emissions as compared to gasoline.

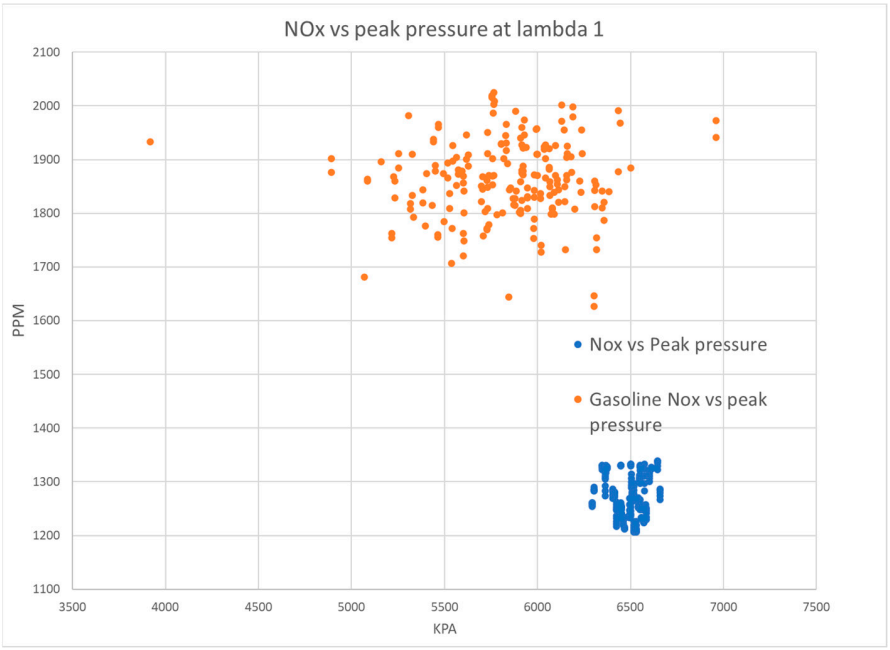

Figure 15. NO_x emission and peak cylinder pressure for hydrogen DI and gasoline DI at a lambda of 1.

Figure 16 depicts NO_x emission at different cylinder pressures and COV_{NO_x} at a lambda of 1.8, the maximum lambda achieved by gasoline. The graph indicates that at this lean condition, gasoline exhibits a higher variation in peak cylinder pressure compared with hydrogen, resulting in a higher COV_{NO_x}.

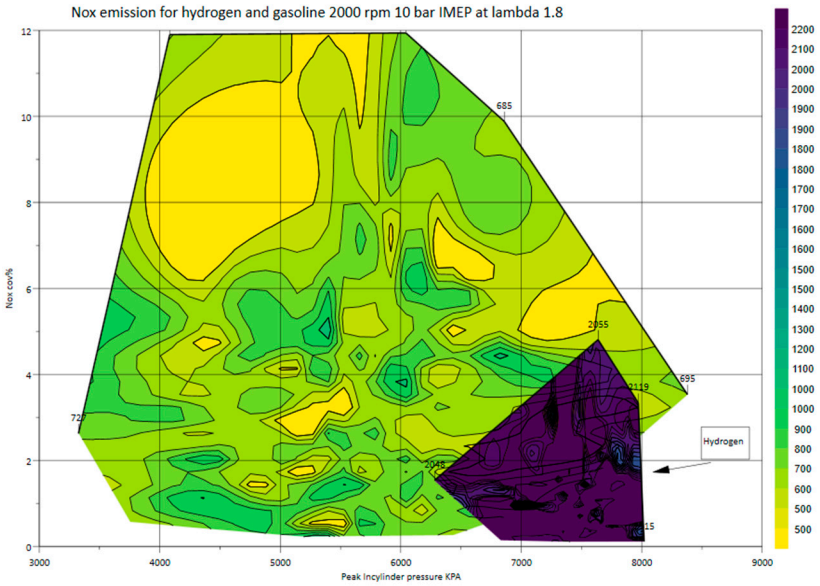

Figure 16. NO_x emission at different peak cylinder pressures and NO_x emission variation for hydrogen DI and gasoline DI at a lambda of 1.8.

Figure 17 shows the results under stoichiometric operating conditions. The data reveal that gasoline has a larger range than hydrogen and is characterised by significantly higher NO_x emissions and greater COV of NO_x at each cycle. Conversely, hydrogen exhibits consistent in-cylinder peak pressure and lower NO_x emissions, with COV of NO_x remaining below 1.7%. Moreover, the data show that higher in-cylinder peak pressure is associated with higher NO_x emissions and greater COV of NO_x, reaching 2.3%. These findings suggest that hydrogen offers considerable advantages over gasoline in terms of its lower NO_x emissions and consistent in-cylinder peak pressure.

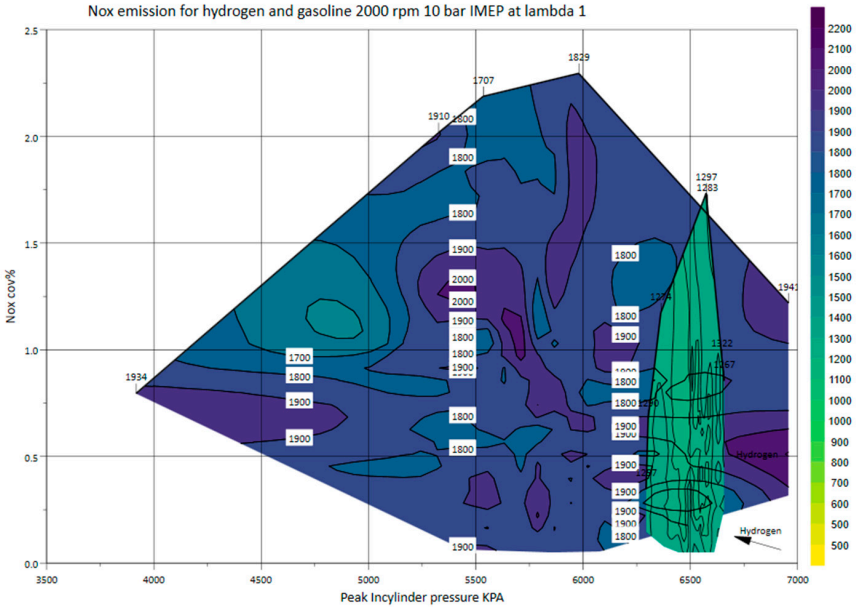

Figure 17. NO_x emission at different peak cylinder pressures and NO_x emission variation for hydrogen DI and gasoline DI at a lambda of 1.

The previous two diagrams directly compared the relationship between in-cylinder peak pressure, NO_x emissions and COV of NO_x for hydrogen and gasoline. These comparisons evaluated the primary NO_x characteristics at a lambda of 1.8 and 1. Given that lambda one is considered the optimal λ for gasoline, it is worthwhile to compare the results at the optimal lambda for hydrogen, which is 2.75. Figure 18 shows the NO_x emission characteristics at lambda 1 for gasoline and lambda 2.75 for hydrogen. The data reveal a higher peak in-cylinder pressure for hydrogen, with nearly zero NO_x emissions. The average NO_x emissions for hydrogen are less than 55 ppm, compared with 1850 ppm for gasoline.

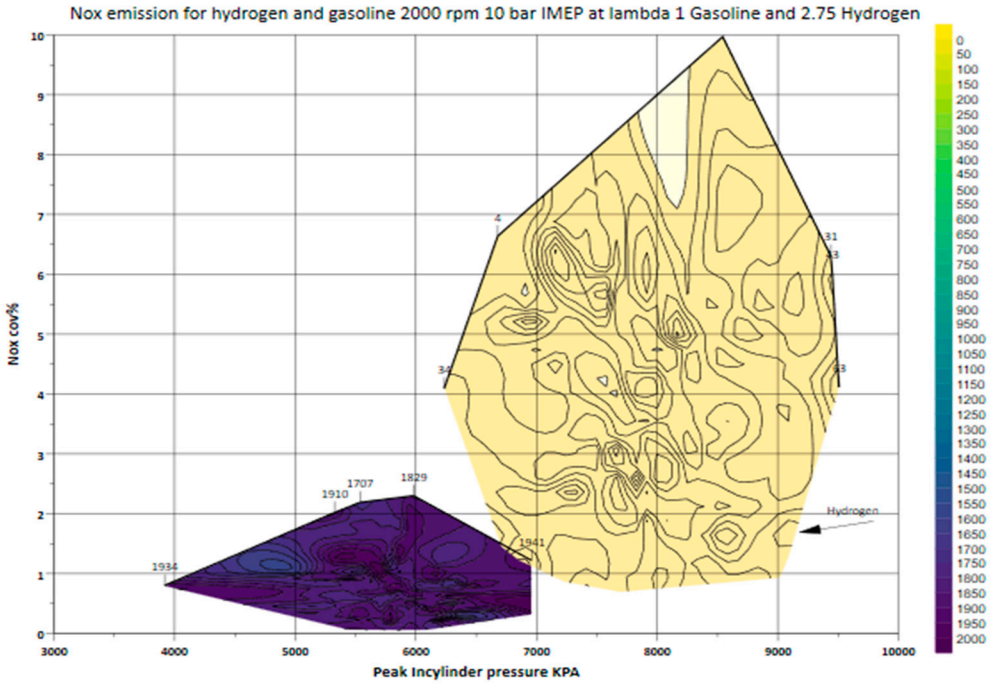

Figure 18. NO_x emission at different peak cylinder pressures and NO_x emission variation for hydrogen DI and gasoline DI at optimum lambda for each fuel.

5. Conclusions

The study explored the primary NO_x emissions characteristics of a hydrogen-fuelled spark ignition (SI) engine designed and optimised for gasoline fuel. The results indicate that using hydrogen fuel has improved combustion stability and reduced cycle-to-cycle variations in peak in-cylinder pressure and NO_x emissions. Additionally, the hydrogen fuel has resulted in higher thermal efficiency and almost zero NO_x emissions at a lambda value of 2.75 without requiring excessive boosting or further modifications to the existing ICE platform.

Hydrogen fuel has a broader operating lambda range compared with gasoline, demonstrating its capability to function efficiently across lambda 1 to nearly lambda 4. This characteristic facilitates the integration of hydrogen fuel in diverse ICE applications. When comparing the NO_x emissions of hydrogen and gasoline at the stoichiometric operation point, it is evident that the former generates fewer emissions, improving the effectiveness of existing after-treatment systems in removing NO_x from the exhaust. When comparing the evolution of NO_x emissions over the crank angle domain for hydrogen DI and PFI systems, it is observed that the PFI system produces slightly less NO_x. This is considered an advantage for existing SI engines that use gasoline PFI and are looking to adopt hydrogen fuel. However, the main limitation of the PFI hydrogen system is the occurrence of backfire when operated with near-stoichiometric mixtures.

The time analysis of the NO_x emissions characteristics reveals that DI hydrogen engine operation produces much higher engine stability and fewer NO_x oscillations than gasoline.

Even at the optimum operation point for gasoline, hydrogen engine operation proved to be more stable with less NO_x emissions and lower NO_x emission fluctuations between cycles.

Author Contributions: Conceptualization, M.M.; Methodology, M.M.; Formal analysis, M.M.; Investigation, M.M.; Resources, M.P. and J.H.; Writing—original draft, M.M.; Writing—review & editing, M.M.; Supervision, X.W., H.Z., J.H. and C.J.; Project administration, H.Z.; Funding acquisition, H.Z. and C.J. All authors have read and agreed to the published version of the manuscript.

Funding: This research was funded by [UKRI] grant number [10014250].

Data Availability Statement: The data presented in this study are available on request from the corresponding author. The data are not publicly available due to privacy and IP protection.

Conflicts of Interest: Author Mark Peckham was employed by the company Cambustion Ltd. Author Jonathan Hall was employed by the company Mahle Powertrain Ltd. The remaining authors declare that the research was conducted in the absence of any commercial or financial relationships that could be construed as a potential conflict of interest.

Definitions/Abbreviations

10% to 90% Burn Duration	Burn Duration
50% MB	Combustion Phasing
AFR/λ	Relative Air-Fuel Ratio
ATDC	After Top Dead Centre
BEV	Battery Electric Vehicle
BTDC	Before Top Dead Centre
CAD	Crank Angle Degree
CO	Carbon Monoxide
CO_2	Carbon Dioxide
COV_{IMEP}	Coefficient of Variation of IMEP
COV_{NOX}	Coefficient of Variation of NO_x
CLD	Chemiluminescence Detector
DAQ	Data Acquisition
DI	Direct Injection
ECU	Electronic Control Unit
EGT	Exhaust Gas Temperature
FCEV	Fuel Cell Electric Vehicle
GHG	Greenhouse Gas
H_2	Hydrogen
HC	Hydrocarbons
ICE	Internal Combustion Engine
IMEP	Indicated Mean Effective Pressure
ITE	Indicated Thermal Efficiency
LIF	Laser-Induced Fluorescence
LNV	Lower Net Value
NH_3	Ammonia
NO_x	Nitrogen Oxides
O_2	Oxygen
PFI	Port Fuel Injection
PLC	Programmable Logic Controller
PM	Particulate Matter
PMEP	Peak Mean Effective Pressure
R_{max}	Pressure Rise Rate
SI	Spark Ignition

Appendix A

Table A1. Table of Uncertainties.

Measurement	Device	Manufacturer	Measurement Range	Linearity/Accuracy
Engine speed	AC Dynamometers (Asynchronous)	Sierra Cp Engineering	0–6000 rpm	±1 rpm
Engine torque	AC Dynamometers (Asynchronous)	Sierra Cp Engineering	−50–500 nm	±0.25% of FS
Clock signal	EB582	Encoder Technology	0–25,000 rpm	0.2 CAD
Hydrogen flow rate	Coriolis flowmeter K000000453	Alicat Scientific	0–10,000 g/h	±0.20% of reading
Intake air mass flow rate	F-106 AI	Bronkhust	4–200 kg/h	±0.2% of reading
In-cylinder pressure	Piezoelectric pressure sensor type 6125C	Kistler	0–30 MPa	≤±0.4% of FS
Intake pressure	Piezoresistive pressure sensor type 4049A	Kistler	0–1 MPa	≤±0.5% of FS
Exhaust pressure	Piezoresistive pressure sensor type 4049B	Kistler	0–1 MPa	≤±0.5% of FS
Oil pressure	PX309-10KGI	omega	0–0.8 MPa	<±0.2% of FS
Temperature	Thermocouple K Type	RS	233–1473 K	≤±2.5 K
Fuel injector current signal	Current probe PR30	LEM	0–20 A	±2 mA
PM emissions	DMS 500	Cambustion	0–5000 PPS	-
CO emissions	MEXA-584L	Horiba	0–12 vol%	≤±1.0% of FS or ±2.0% of readings
CO_2 emissions	MEXA-584L	Horiba	0–20 vol%	≤±1.0% of FS or ±2.0% of readings
O2	MEXA-584L	Horiba	0–25 vol%	≤±1.0% of FS or ±2.0% of readings
THC emissions	Rotork Analysis Model 523	Signal	0–5000 ppm	≤±1.0% of FS or ±2.0% of readings
NO/NO_2 emissions	CLD 150 (Heated Chemiluminescence Detector)	Cambustion	0–500 ppm or 0–10 k ppm	≤±1.0% of FS or ±2.0% of readings
H2 slip emissions	Air sens500	V&F	0–5000 ppm or 0–100% vol	0.5% of fs or 1%vol

References

1. Revision of CO2 Emission Performance Standards for Cars and Vans, as Part of the European Green Deal-Q2 2021. Available online: https://www.europarl.europa.eu/legislative-train/theme-a-european-green-deal/file-co2-emission-standards-for-cars-and-vans-post-euro6vi-emission-standards (accessed on 22 March 2022).
2. Office of the Federal Register, National Archives and Records Administration. DCPD-202100640—Executive Order 14037-Strengthening American Leadership in Clean Cars and Trucks. August 2021. Available online: https://www.govinfo.gov/app/details/DCPD-202100640 (accessed on 11 December 2023).
3. Huang, R.-J.; Zhang, Y.; Bozzetti, C.; Ho, K.-F.; Cao, J.-J.; Han, Y.; Daellenbach, K.R.; Slowik, J.G.; Platt, S.M.; Canonaco, F.; et al. High secondary aerosol contribution to particulate pollution during haze events in China. *Nature* **2014**, *514*, 218–222. [CrossRef]
4. Lelieveld, J.; Evans, J.S.; Fnais, M.; Giannadaki, D.; Pozzer, A. The contribution of outdoor air pollution sources to premature mortality on a global scale. *Nature* **2015**, *525*, 367–371. [CrossRef] [PubMed]
5. Jones, L.; Stevens, C.; Rowe, E.; Payne, R.; Caporn, S.; Evans, C.; Field, C.; Dale, S. Can on-site management mitigate nitrogen deposition impacts in non-wooded habitats? *Biol. Conserv.* **2016**, *212*, 464–475. [CrossRef]

6. Bobbink, R.; Hicks, K.; Galloway, J.; Spranger, T.; Alkemade, R.; Ashmore, M.; Bustamante, M.; Cinderby, S.; Davidson, E.; Dentener, F.; et al. Global assessment of nitrogen deposition effects on terrestrial plant diversity: A synthesis. *Ecol. Appl.* **2010**, *20*, 30–59. [CrossRef]
7. Galloway, J.N.; Townsend, A.R.; Erisman, J.W.; Bekunda, M.; Cai, Z.; Freney, J.R.; Martinelli, L.A.; Seitzinger, S.P.; Sutton, M.A. Transformation of the Nitrogen Cycle: Recent Trends, Questions, and Potential Solutions. *Science* **2008**, *320*, 889–892. [CrossRef]
8. Howarth, R.W.; Sharpley, A.; Walker, D. Sources of Nutrient Pollution to Coastal Waters in the United States: Implications for Achieving Coastal Water Quality Goals. *Estuaries* **2002**, *25*, 656–676. Available online: http://www.jstor.org/stable/1353025 (accessed on 23 March 2022). [CrossRef]
9. Mohamed, M.; Zhao, H.; Harrington, A.; Hall, J. *Experimental Investigation of Combustion Characteristics, Performance, and Emissions of a Spark Ignition Engine with 2ndGeneration Bio-Gasoline and Ethanol Fuels*; SAE Technical Papers; SAE International: Warrendale, PA, USA, 2023. [CrossRef]
10. Harrington, A.; Hall, J.; Cooper, A.; Bassett, M.; Hiett, N.; Richardson, D.; Martens, A.; Sapsford, S. *Technical Assessment of the Feasibility of the Use of Bio-Gasoline as a Drop-In Gasoline Fossil Fuel Replacement*; SAE Technical Papers; SAE International: Warrendale, PA, USA, 2022. [CrossRef]
11. Iodice, P.; Amoresano, A.; Langella, G. A review on the effects of ethanol/gasoline fuel blends on NOX emissions in spark-ignition engines. *Biofuel Res. J.* **2021**, *8*, 1465–1480. [CrossRef]
12. Kumar, A.; Khatri, D.S.; Babu, M.K.G. *An Investigation of Potential and Challenges with Higher Ethanol-Gasoline Blend on a Single Cylinder Spark Ignition Research Engine*; SAE Technical Papers; SAE International: Warrendale, PA, USA, 2009. [CrossRef]
13. Harrington, A.; Hall, J.; Bassett, M.; Lu, E.; Zhao, H. *Combustion Characteristics and Exhaust Emissions of a Direct Injection SI Engine with Pure Ethanol and Methanol in Comparison to Gasoline*; SAE Technical Papers; SAE International: Warrendale, PA, USA, 2022. [CrossRef]
14. Verhelst, S.; Turner, J.W.; Sileghem, L.; Vancoillie, J. Methanol as a fuel for internal combustion engines. *Prog. Energy Combust. Sci.* **2019**, *70*, 43–88. [CrossRef]
15. Wang, L.; Li, H.; Huang, Z.; Wang, L.; Chen, W. Impact of hydrogen direct injection on engine combustion and emissions in a GDI engine. *Adv. Mech. Eng.* **2023**, *15*, 16878132231189117. [CrossRef]
16. Sharma, S.; Ghoshal, S.K. Hydrogen the future transportation fuel: From production to applications. *Renew. Sustain. Energy Rev.* **2015**, *43*, 1151–1158. [CrossRef]
17. Bose, P.K.; Maji, D. An experimental investigation on engine performance and emissions of a single cylinder diesel engine using hydrogen as inducted fuel and diesel as injected fuel with exhaust gas recirculation. *Int. J. Hydrogen Energy* **2009**, *34*, 4847–4854. [CrossRef]
18. Cornelius, W.; Huellmantel, L.W.; Mitchell, H.R. *Ammonia as an Engine Fuel*; SAE Transactions; SAE International: Warrendale, PA, USA, 1966; Volume 74, pp. 300–326. Available online: http://www.jstor.org/stable/44460524 (accessed on 12 March 2022).
19. Gray, J.T.; Dimitroff, E.; Meckel, N.T.; Quillian, R.D. *Ammonia Fuel—Engine Compatibility and Combustion*; SAE Transactions; SAE International: Warrendale, PA, USA, 1967; Volume 75, pp. 785–807. Available online: http://www.jstor.org/stable/44563675 (accessed on 19 April 2023).
20. Tornatore, C.; Marchitto, L.; Sabia, P.; De Joannon, M. Ammonia as Green Fuel in Internal Combustion Engines: State-of-the-Art and Future Perspectives. *Front. Mech. Eng.* **2022**, *8*, 944201. [CrossRef]
21. Dimitriou, P.; Javaid, R. A review of ammonia as a compression ignition engine fuel. *Int. J. Hydrogen Energy* **2020**, *45*, 7098–7118. [CrossRef]
22. Tang, X.; Kabat, D.M.; Natkin, R.J.; Stockhausen, W.F.; Heffel, J. *Ford P2000 Hydrogen Engine Dynamometer Development*; SAE Technical Papers; SAE International: Warrendale, PA, USA, 2002. [CrossRef]
23. Fayaz, H.; Saidur, R.; Razali, N.; Anuar, F.S.; Saleman, A.R.; Islam, M.R. An overview of hydrogen as a vehicle fuel. *Renew. Sustain. Energy Rev.* **2012**, *16*, 5511–5528. [CrossRef]
24. Stępień, Z. A Comprehensive Overview of Hydrogen-Fueled Internal Combustion Engines: Achievements and Future Challenges. *Energies* **2021**, *14*, 6504. [CrossRef]
25. Jilakara, S.; Vaithianathan, J.V.; Natarajan, S.; Ramakrishnan, V.R.; Subash, G.; Abraham, M.; Unni, J.K.; Das, L.M. An Experimental Study of Turbocharged Hydrogen Fuelled Internal Combustion Engine. *SAE Int. J. Engines* **2015**, *8*, 314–325. Available online: http://www.jstor.org/stable/26277943 (accessed on 14 April 2021). [CrossRef]
26. Milojević, S.; Savić, S.; Marić, D.; Stopka, O.; Krstić, B.; Stojanović, B. Correlation between Emission and Combustion Characteristics with the Compression Ratio and Fuel Injection Timing in Tribologically Optimized Diesel Engine. *Teh. Vjesn.* **2022**, *29*, 1210–1219. [CrossRef]
27. Milojević, S.; Glišović, J.; Savić, S.; Bošković, G.; Bukvić, M.; Stojanović, B. Particulate Matter Emission and Air Pollution Reduction by Applying Variable Systems in Tribologically Optimized Diesel Engines for Vehicles in Road Traffic. *Atmosphere* **2024**, *15*, 184. [CrossRef]
28. Safari, H.; Jazayeri, S.A.; Ebrahimi, R. Potentials of NOX emission reduction methods in SI hydrogen engines: Simulation study. *Int. J. Hydrogen Energy* **2009**, *34*, 1015–1025. [CrossRef]
29. Deng, J.; Ma, F.; Li, S.; He, Y.; Wang, M.; Jiang, L.; Zhao, S. Experimental study on combustion and emission characteristics of a hydrogen-enriched compressed natural gas engine under idling condition. *Int. J. Hydrogen Energy* **2011**, *36*, 13150–13157. [CrossRef]

30. Shang, W.; Yu, X.; Shi, W.; Xing, X.; Guo, Z.; Du, Y.; Liu, H.; Wang, S. Effect of exhaust gas recirculation and hydrogen direct injection on combustion and emission characteristics of a n-butanol SI engine. *Int. J. Hydrogen Energy* **2020**, *45*, 17961–17974. [CrossRef]
31. Jamrozik, A.; Grab-Rogaliński, K.; Tutak, W. Hydrogen effects on combustion stability, performance and emission of diesel engine. *Int. J. Hydrogen Energy* **2020**, *45*, 19936–19947. [CrossRef]
32. Sandalci, T.; Karagöz, Y. Experimental investigation of the combustion characteristics, emissions and performance of hydrogen port fuel injection in a diesel engine. *Int. J. Hydrogen Energy* **2014**, *39*, 18480–18489. [CrossRef]
33. Mohamed, M.; Longo, K.; Zhao, H.; Hall, J.; Harrington, A. *Hydrogen Injection Insights: A Comprehensive Experimental Examination of Port Fuel Injection and Direct Injection*; SAE International: Warrendale, PA, USA, 2024.
34. Mohamed, M.; Mirshahi, M.; Jiang, C.; Zhao, H.; Harrington, A.; Hall, J. Hydrogen Injection Position Impact: Experimental Analysis of Central Direct Injection and Side Direct Injection in Engines. *SAE Int. J. Engines* **2024**, *17*, 669–687. [CrossRef]
35. Fast Response Portable NO and NO2 Analyzer | CLD50. Available online: https://www.cambustion.com/products/engine-exhaust-emissions/nox-analyzers/cld50-ambient-and-engine-nox (accessed on 13 December 2023).
36. Mohamed, M.; Biswal, A.; Wang, X.; Zhao, H.; Harrington, A.; Hall, J. Unveiling the Potential of Hydrogen in a Downsized Gasoline Direct Injection Engine Performance and Emissions Experimental Study. *SAE Int. J. Fuels Lubr.* **2024**, *17*, 3. [CrossRef]